J|A|C|S
ARTICLES

Published on Web 07/07/2010

Modification of the Optoelectronic Properties of Membranes via Insertion of Amphiphilic Phenylenevinylene Oligoelectrolytes

Logan E. Garner,[†] Juhyun Park,[‡] Scott M. Dyar,[†] Arkadiusz Chworos,[†] James J. Sumner,[§] and Guillermo C. Bazan*,[†]

Department of Chemistry and Biochemistry, University of California, Santa Barbara, California 93106, U.S. Army Research Laboratory, Sensors and Electron Devices Directorate, Adelphi, Maryland 20783, and School of Chemical Engineering and Materials Science, Chung-Ang University, 221 Heukseok-Dong, Dongjak-Gu, Seoul, Korea

Received February 24, 2010; E-mail: bazan@chem.ucsb.edu

Abstract: We report on the modification of membranes by incorporation of phenylenevinylene oligoelectrolytes with the goal of tailoring their optical and electronic properties and their applications. A water-soluble distyrylstilbene oligoelectrolyte (**DSSN**+), capped at each end with nitrogen bound, terminally charged pendant groups, was synthesized. The photophysical and solvatochromatic properties of **DSSN**+ and the shorter distyrylbenzene analogue **DSBN**+ were probed and found to be useful for characterizing insertion into membranes based on phospholipid vesicle systems. A combination of UV/visible absorbance and photoluminescence spectroscopies, together with confocal microscopy, were employed to confirm membrane incorporation. Examination of the emission intensity profile in stationary multilamellar vesicles obtained with a polarized excitation source provides insight into the orientation of these chromophores within lipid bilayers and indicates that these molecules are highly ordered, such that the hydrophobic electronically delocalized region positions within the inner membrane with the long molecular axis perpendicular to the bilayer plane. Cyclic voltammetry experiments provide evidence that **DSSN**+ and **DSBN**+ facilitate transmembrane electron transport across lipid bilayers supported on glassy carbon electrodes. Additionally, the interaction with living microorganisms was probed. Fluorescence imaging indicates that **DSSN**+ and **DSBN**+ preferentially accumulate within cell membranes. Furthermore, notable increases in yeast microbial fuel cell performance were observed when employing **DSSN**+ as the electron transport mediator.

Introduction

Conjugated oligomers can be described by a select number of repeat units extracted from a polymer containing an electronically π-delocalized backbone. Homologous progressions of these molecules, and related systems with extended electronic delocalization, have been useful in fundamental studies with a focus on understanding how molecular connectivity influences optical and electronic properties and in the development of emerging technologies.[1] One well-appreciated opportunity involves integration as the semiconducting component in field effect transistors (FETs) relevant for plastic electronics.[2] A wide range of structural variations have been designed, developed, and incorporated into FETs via different deposition methods.[3] The accumulated effort has yielded insight not only into device optimization but also on how weak intermolecular forces can be coordinated to yield desirable morphologies at interfaces and how intermolecular arrangements mediate charge carrier transport.[4] More recently, thin films of conjugated oligomers bearing pendant groups with ionic functionalities, i.e., conjugated oligoelectrolytes (COEs), were demonstrated to be effective for reducing charge injection barriers at metal/organic interfaces.[5]

[†] University of California.
[‡] Chung-Ang University.
[§] U.S. Army Research Laboratory.

(1) (a) Martin, R. E.; Diederich, F. *Angew. Chem., Int. Ed.* **1999**, *38*, 1350–1377. (b) *Electronic Materials: The Oligomer Approach*; Mullen, K., Wegner, G., Eds.; Wiley: Weinheim, 1998. (c) Tour, J. M. *Chem. Rev.* **1996**, *96*, 537–553.

(2) (a) Brédas, J.-L.; Beljonne, D.; Coropceanu, V.; Cornil, J. *Chem. Rev.* **2004**, *104*, 4971–5003. (b) Facchetti, A. *Mater. Today* **2007**, *10*, 28–37. (c) Facchetti, A.; Mushrush, M.; Yoon, M.-H.; Hutchison, G. R.; Ratner, M. A.; Marks, T. *J. Am. Chem. Soc.* **2004**, *126*, 13859–13874. (d) Katz, H. E.; Bao, Z.; Gilat, S. L. *Acc. Chem. Res.* **2001**, *34*, 359–369. (e) Murphy, A. R.; Fréchet, J. M. *Chem. Rev.* **2007**, *107*, 1066–1096. (f) Yamishita, Y. *Sci. Technol. Adv. Mater.* **2009**, *10*, 1–9. (g) Yasuda, T.; Ooi, H.; Morita, J.; Akama, Y.; Minoura, K.; Funahashi, M.; Shimomura, T.; Kato, T. *Adv. Funct. Mater.* **2009**, *19*, 411–419.

(3) (a) Bao, Z.; Rogers, J. A.; Katz, H. E. *J. Mater. Chem.* **1999**, *9*, 1895–1904. (b) Briseno, A. L.; Roberts, M.; Ling, M.-M.; Moon, H.; Nemanick, E. J.; Bao, Z. *J. Am. Chem. Soc.* **2006**, *128*, 3880–3881. (c) Chandekar, A.; Whitten, J. E. *Appl. Phys. Lett.* **2007**, *91*, 113103. (d) Drolet, N.; Morin, J.-F.; Leclerc, N.; Wakim, S.; Tao, Y.; Leclerc, M. *Adv. Funct. Mater.* **2005**, *15*, 1671–1682. (e) Geens, W.; Tsamouras, D.; Poortmans, J.; Hadziioannou, G. *Synth. Met.* **2001**, *122*, 191–194. (f) Jurchescu, O. D.; Subramanian, S.; Kline, R. J.; Hudson, S. D.; Anthony, J. E.; Jackson, T. N.; Gundlach, D. J. *Chem. Mater.* **2008**, *20*, 6733–6737. (g) Maulden, C. E.; Puntambekar, K.; Murphy, A. R.; Liao, F.; Subramanian, V.; Fréchet, J. M. J.; DeLongchamp, D. M.; Fischer, D. A.; Toney, M. F. *Chem. Mater.* **2009**, *21*, 1927–1938.

(4) (a) Coropceanu, V.; Cornil, J.; de Silva, D. A.; Olivier, Y.; Silbey, R.; Brédas, J.-L. *Chem. Rev.* **2007**, *107*, 926–952. (b) Fichou, D. *J. Mater. Chem.* **2000**, *10*, 571–588. (c) Hutchison, G. R.; Ratner, M. A.; Marks, T. J. *J. Am. Chem. Soc.* **2005**, *127*, 16866–16881. (d) Leclère, Ph.; Surin, M.; Viville, P.; Lazzaroni, R.; Kilbinger, A. F. M.; Henze, O.; Feast, W. J.; Cavallini, M.; Biscarini, F.; Schenning, A. P. H. J.; Meijer, E. W. *Chem. Mater.* **2004**, *16*, 4452–4466.

(5) Yang, R.; Xu, Y.; Dang, X.-D.; Nguyen, T.-Q.; Cao, Y.; Bazan, G. C. *J. Am. Chem. Soc.* **2008**, *130*, 3282–3283.

10.1021/ja1016156

While more than one mechanism may be operating, for example, ion motion and/or the formation of a spontaneously aligned dipole layer, the simplicity of incorporating COE injection layers via solution methods opens the opportunity to reduce the operating voltages of polymer-based light emitting diodes.

Several structural types of conjugated oligomers have also been used in molecular transconductance studies that assess charge transfer across a single or a few molecules. For instance, comparison of oligophenylenevinylene (OPV) and oligophenyleneethynylene (OPE) structures that span two gold contacts reveals better conductance across the OPV framework, relative to OPE.[6] Such experimental findings are corroborated by theoretical calculations and have revealed that structural parameters that affect HOMO−LUMO energy levels, such as planarity and bond length alternation, influence charge transport efficiency.[7,8] Electrochemical measurements have also been used to demonstrate that OPVs of various lengths facilitate tunneling between a gold surface and a tethered redox species.[9] The work to date regarding single molecule transconductance has offered much insight into the factors that influence charge transport and has laid the foundation for the design and development of molecular wires that may play a role as charge transporting components in new technologies.

Oligomers broadly described by a D−π−D structure, where D is an electron-donating group and π refers to a π-delocalized linker, have been immensely instructional for understanding and optimizing two photon absorption processes in organic materials. Some of these molecular systems have been utilized for three-dimensional fabrication[10] and for two-photon microscopy of biological systems.[11−13] Molecules possessing D−π−D structures typically undergo intramolecular charge transfer excitation that results in large two-photon absorption cross sections.[14] One specific example is the molecule 1,4-bis(4′-(*N*,*N*-bis(6″-(*N*,*N*,*N*-trimethylammonium)hexyl)amino)-styryl)benzene tetraiodide (**DSBN**+), the structure of which is shown in Scheme 1. This molecule incorporates charged groups that increase solubility in highly polar organic solvents and water. The distyrylbenzene (DSB) conjugated region is capped at each end with two nitrogen-bound, six-carbon pendant groups containing terminal quaternary ammonium salts. By examination of optical properties in different solvents, and in combination with neutral derivatives, it is possible to examine how the dielectric constant of the medium perturbs linear and two-photon spectral responses.[15] These studies have highlighted the challenges in predicting a priori how the molecular features and the environment combine to yield different optical properties. It was also found that molecules such as **DSBN**+ display much larger emission quantum efficiencies and two-photon absorption cross sections upon incorporation into micelles from an aqueous environment.[16] Association with the interior of the micelle is likely a consequence of the hydrophobic DSB framework.

Scheme 1. Structure of OPV Oligoelectrolytes

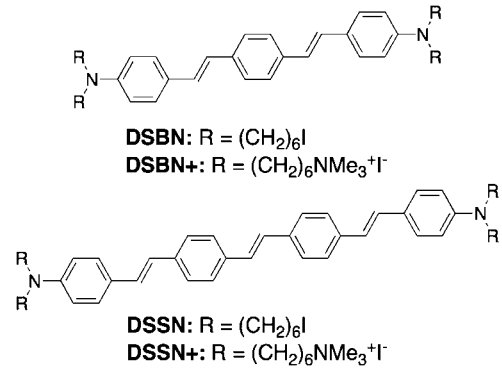

On the basis of the background delineated above and a consideration of the molecular dimensions of **DSBN**+, it occurred to us that it would be possible to intercalate this molecule into lipid bilayer membranes in an ordered orientation. A schematic cartoon of the general concept is provided in Figure 1. The dependence of optical features as a function of the medium provides a useful characterization handle. Furthermore, the precedence of using OPVs in single-molecule charge transport measurements argues in favor of these molecules being able to mediate transmembrane charge transfer.

This manuscript is organized as follows. We begin with the synthesis of a longer water-soluble oligoelectrolyte analogue of **DSBN**+, namely 4,4′-bis(4′-(*N*,*N*-bis(6″-(*N*,*N*,*N*-trimethylammonium)hexyl)amino)-styryl)stilbene tetraiodide (**DSSN**+ in Scheme 1). Successful incorporation into lipid bilayer vesicles and membranes is demonstrated by a variety of techniques

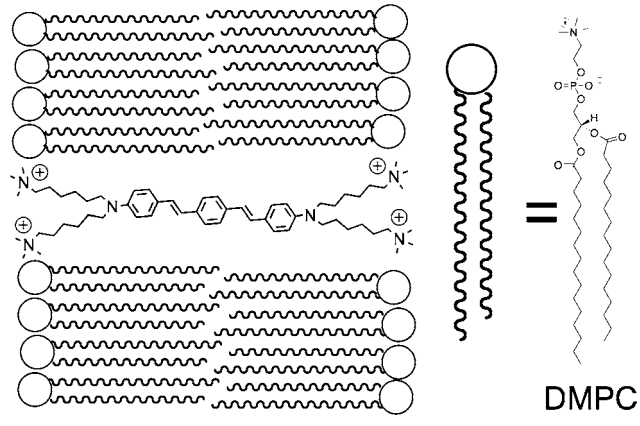

Figure 1. Cartoon representation of a **DSBN**+ modified lipid bilayer depicting the predicted orientation when intercalated within a phospholipid bilayer. The long molecular axis is normal to the plane of the membrane with the hydrophobic conjugated region within the nonpolar inner membrane and the polar pendant group terminals oriented outward toward the polar aqueous environment on either side of the lipid bilayer.

(6) Huber, R.; González, M. T.; Wu, S.; Langer, M.; Grunder, S.; Horhoiu, V.; Mayor, M.; Bryce, M. R.; Wang, C.; Jitchati, R.; Schönenberger, C.; Calame, M. *J. Am. Chem. Soc.* **2008**, *130*, 1080–1084.
(7) Sachs, S. B.; Dudek, S. P.; Hsung, R. P.; Sita, L. R.; Smalley, J. F.; Newton, M. D.; Feldberg, S. W.; Chidsey, C. E. D. *J. Am. Chem. Soc.* **1997**, *119*, 10563–10564.
(8) (a) Kushmerick, J. G.; Pollack, S. K.; Yang, J. C.; Naciri, J.; Holt, D. B.; Ratner, M. A.; Shashidhar, R. *Ann. N.Y. Acad. Sci.* **2003**, *1006*, 277–290. (b) Kushmerick, J. G.; Holt, D. B.; Pollack, S. K.; Ratner, M. A.; Yang, J. C.; Schull, T. L.; Naciri, J.; Moore, M. H.; Shashidhar, R. *J. Am. Chem. Soc.* **2002**, *124*, 10654–10655. (c) Yin, X.; Liu, H.; Zhao, J. *J. Chem. Phys.* **2006**, *125*, 094711.
(9) (a) Dudek, S. P.; Sikes, H. D.; Chidsey, C. E. D. *J. Am. Chem. Soc.* **2001**, *123*, 8033–8038. (b) Sikes, H. D.; Smalley, J. F.; Dudek, S. P.; Cook, A. R.; Newton, M. D.; Chidsey, C. E. D.; Feldberg, S. W. *Science* **2001**, *291*, 1519–1523.
(10) Zhou, W. H.; Kuebler, S. M.; Braun, K. L.; Yu, T. Y.; Cammack, J. K.; Ober, C. K.; Perry, J. W.; Marder, S. R. *Science* **2002**, *296*, 1106–1109.
(11) So, P. T. C.; Dong, C. Y.; Masters, B. R.; Berland, K. M. *Annu. Rev. Biomed. Eng.* **2000**, *02*, 399.
(12) (a) Centonze, V. E.; White, J. G. *Biophys. J.* **1998**, *75*, 2015–2024. (b) Periasamy, A.; Skoglund, P.; Noakes, C.; Keller, R. *Microsc. Res. Technol.* **1999**, *47*, 172–181. (c) Zipfel, W. R.; Williams, R. M.; Webb, M. W. *Nat. Biotechnol.* **2003**, *21*, 1369–1377.
(13) Xu, C.; Williams, R. M.; Zipfel, W.; Webb, M. W. *Bioimaging* **1996**, *4*, 198–207.
(14) Albota, M.; et al. *Science* **1998**, *281*, 1653–1656.

Scheme 2. Synthetic Procedures for Preparation of **DSSN** and **DSSN**+[a]

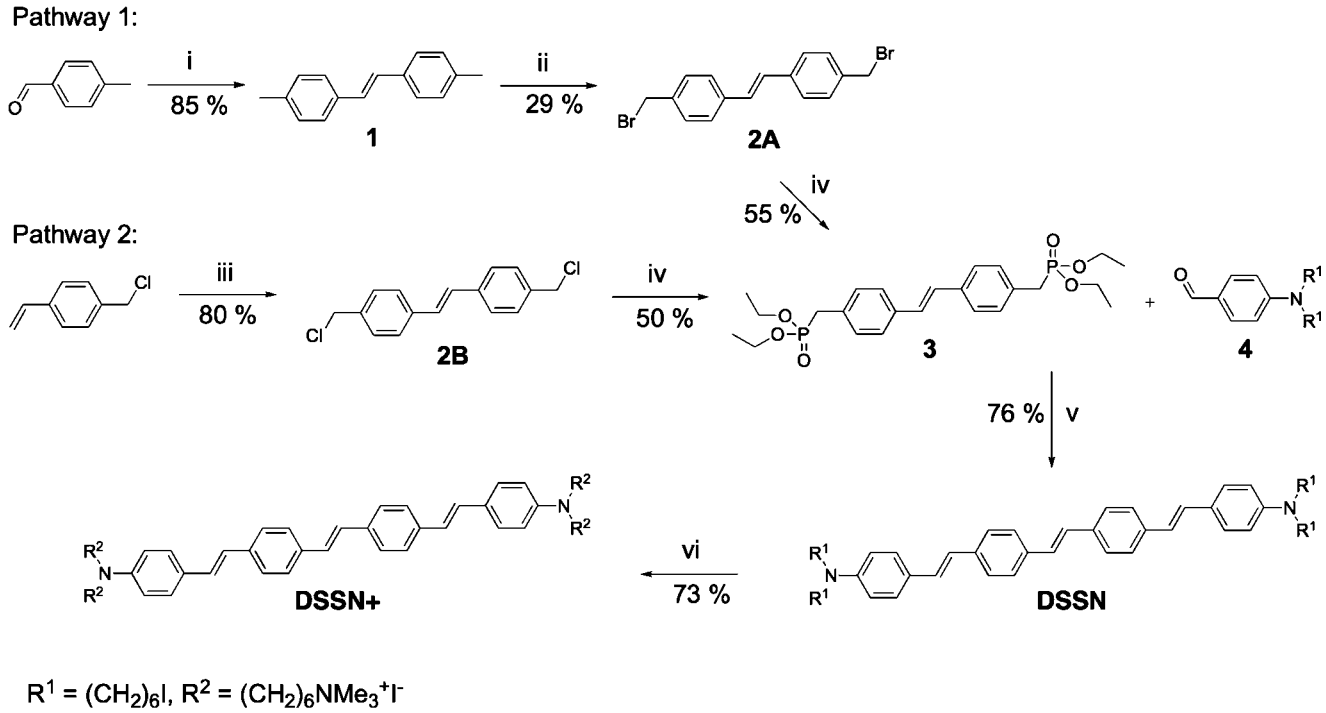

[a] Reagents and conditions: (i) Zn, $TiCl_4$, THF, 24 h. (ii) NBS, AIBN, benzene, reflux, 24 h. (iii) $C_{46}H_{65}Cl_2N_2PRu$ (Grubbs catalyst, second generation), CH_2Cl_2, reflux, 24 h. (iv) $P(OEt)_3$ neat, reflux, 24 h. (v) ^{t}BuONa, THF, RT, 24 h. (vi) a. NMe_3, THF, RT, 24 h; b. NMe_3, MeOH, RT, 24 h.

including confocal microscopy. Polarized excitation sources demonstrate that **DSBN**+ and **DSSN**+ are immobilized within the bilayers in an orientation such that the hydrophobic long molecular axis is perpendicular to the plane of the membrane and the polar pendant group terminals are positioned at the outer surfaces. Favorable interaction with living systems revealed spontaneous insertion within cell membranes. Results obtained from cyclic voltammetry blocking experiments are in agreement with significant improvements of transmembrane electron transport. Lastly, notable improvements in yeast microbial fuel cell performance were observed when employing **DSBN**+ and **DSSN**+ as electron transport mediators. These findings provide the basis for improving charge extraction from living microorganisms and for developing new membrane-specific optical labels for a variety of imaging techniques.

Results and Discussion

Synthesis and Characterization. Compound **DSBN**+ was prepared as previously reported.[15] Scheme 2 shows the synthesis of **DSSN**+. This route is based upon the assembly of the desired end-capped π-system by coupling a bis(methylene)phosphonate (for example, **3** in Scheme 2) with the amino-functionalized benzaldehyde **4**[15] via a *trans*-selective Horner−Wadsworth−Emmons reaction. Compound **3** may be accessed via two different pathways. The three-step pathway (Pathway 1, Scheme 2) begins with preparation of **1** in good yield via a McMurry coupling of *p*-tolualdehyde followed by a low-yielding (29%) Wohl−Ziegler radical bromination that affords **2A**.[17] The desired bisphosphonate **3** can then be generated by an Arbuzov reaction. Alternatively, **3** can be prepared in two steps (Pathway 2, Scheme 2) beginning with the metathesis condensation of 4-vinylbenzylchloride to yield **2B**, followed by an Arbuzov reaction. The second pathway removes one step, while effectively circumventing a low-yielding radical bromination at the negligible cost of a slightly lower reaction yield (50% and 55% yield of **3** for the two- and three-step pathways, respectively). As stated above, a subsequent Horner−Wadsworth−Emmons reaction affords the neutral chromophore **DSSN** in reasonable yield (76%). Preparation of **DSSN**+ (73% yield) was completed by quaternization of **DSSN** using trimethylamine.

Each synthetic target and intermediate was characterized by ^{1}H and ^{13}C NMR spectroscopy, mass spectrometry, and elemental analysis. Evidence indicating all-*trans* conformations of **DSSN** and **DSSN**+ was provided by ^{1}H NMR spectroscopy. Signals corresponding to protons of the center vinylic linkage are observed as a singlet, indicating a high degree of molecular symmetry, while signals corresponding to protons of the outer vinylic linkages are observed as a doublet with a coupling constant indicative of a *trans* conformation ($J = \sim$16 Hz).

Optical Characterization. General photophysical and solvatochromatic features of the neutral (**DSSN**, **DSBN**) and charged (**DSSN**+, **DSBN**+) versions of each chromophore were probed by using UV−vis absorption and photoluminescence (PL) spectroscopies. As expected, these structural analogues exhibit similar sensitivities to the polarity of the surrounding medium. Table 1 shows a summary and comparison of the spectral characteristics for the neutral and charged versions of each chromophore in solvents of varying polarities. Figure 2 shows the corresponding PL spectra. General trends expressed by both structural analogue pairs are as follows: absorbance maxima (λ_{abs}) occur in the 406−436 nm range and exhibit relatively small shifts in different solvents. Large hypsochromic shifts in PL maxima (λ_{em}) and increased quantum efficiencies (η) are

(15) Woo, H. Y.; Liu, B.; Kohler, B.; Korystov, D.; Mikhailovsky, A.; Bazan, G. C. *J. Am. Chem. Soc.* **2005**, *127*, 14721–14729.
(16) Woo, H. Y.; Korystov, D.; Mikhailovsky, A.; Nguyen, T.-Q.; Bazan, G. C. *J. Am. Chem. Soc.* **2005**, *127*, 13794–13795.
(17) Feast, W. J.; Lovenich, P. W.; Puschmann, H.; Taliani, C. *Chem. Commun.* **2001**, 505–506.

Table 1. Summary of UV−vis and PL Spectra

	toluene		THF		DMSO		water	
	λ_{abs} (ε_{max})[a]	λ_{em} (η)[b]	λ_{abs} (ε_{max})	λ_{em} (η)	λ_{abs} (ε_{max})	λ_{em} (η)	λ_{abs} (ε_{max})	λ_{em} (η)
DSSN	425 (10.7)	476 (0.95)	426 (10.6)	526 (0.89)	436 (9.6)	602 (0.73)		
DSSN+					435 (9.8)	596 (0.71)	412 (6.6)	594 (0.06)
DSBN	410 (8.4)	454 (0.98)	410 (8.5)	466 (0.92)	419 (7.8)[c]	516 (0.81)		
DSBN+					419 (8.2)	511 (0.86)	406 (6.0)	566 (0.33)

[a] Molar extinction coefficients (ε_{max}) were measured at λ_{max} and are reported in units of L mol^{-1} cm^{-1} × 10^{-4}. [b] Quantum efficiency (η) values were measured relative to a fluorescein standard at pH 12. [c] ε_{max} value abstracted from ref 15.

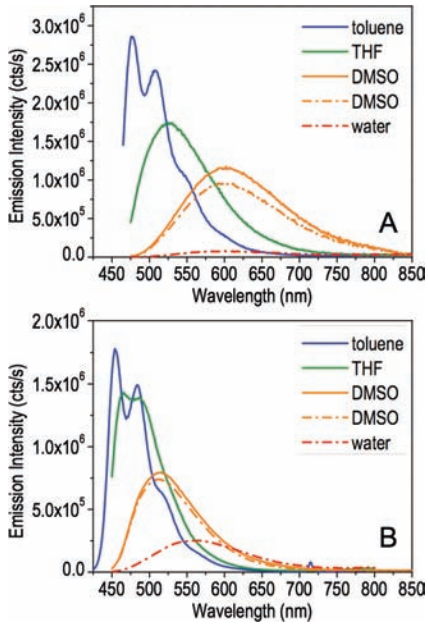

Figure 2. PL spectra of 5−7 μM **DSSN** (A, solid lines), **DSSN+** (A, dashed lines), **DSBN** (B, solid lines), and **DSBN+** (B, dashed lines) in various solvents. Peak areas shown are proportional to η values. General trends exhibited by both chromophores: λ_{em} decreases and η increases with decreasing solvent polarity. Excitation wavelengths were chosen to match the optical density of the fluorescein reference sample.

observed as the solvent polarity decreases. Compared to the distyrylbenzene chromophore (**DSBN** and **DSBN+**), the distyrylstilbene counterpart (**DSSN** and **DSSN+**) has red-shifted λ_{abs} and λ_{em} and a larger molar extinction coefficient (ε_{max}), consistent with its more extended conjugation length and greater size.[18] It is important to note that when comparing the solvatochromatic properties of a given neutral and charged chromophore pair the difference in pendant group terminals (alkyliodide in **DSSN** and **DSBN** vs trimethyl ammonium iodide in **DSSN+** and **DSBN+**) has a negligible effect on the electronic structure of the chromophore.[15] This conclusion is supported by the nearly identical UV−vis and PL features of each structural analogue pair when dissolved in DMSO (Table 1, Figure 2).

As seen in Figure 2, the λ_{em} values of each chromophore exhibit a ∼110−120 nm hypsochromic shift as the solvent is shifted from polar (λ_{em} = 594 and 566 nm in water for **DSSN+** and **DSBN+**, respectively) to nonpolar (λ_{em} = 476 and 454 nm in toluene for **DSSN** and **DSBN**, respectively). This shift is accompanied by the appearance of vibronic structure.[19] The η values of each analogue are similar for a given solvent and are considerably greater in toluene (0.95 and 0.98 for **DSSN** and **DSBN**, respectively) than in water (0.06 and 0.33 for **DSSN+** and **DSBN+**, respectively). Figure 2 shows the PL spectra of **DSSN**/**DSSN+** (Figure 2A) and **DSBN**/**DSBN+** (Figure 2B); peak areas are proportional to the magnitude of η in Table 1. The difference in η values of **DSSN+** and **DSBN+** in water may be due to a greater degree of **DSSN+** aggregation caused by its larger hydrophobic component, which may lead to increased self-quenching.[20,21]

Incorporation of COEs into Lipid Bilayers. A model vesicle system was chosen to examine the incorporation of **DSBN+** and **DSSN+** into phospholipid bilayers, develop a characterization methodology, and ascertain molecular orientation. Vesicles are excellent model systems for membranes due to their ease of formation via self-assembly, structural integrity, large surface area, and high degree of order with respect to spherical shape and orientation of the molecular constituents.[22] The specific lipids employed were 1,2-dimyristoyl-*sn*-glycero-3-phosphocholine (DMPC) and 1,2-dipalmitoyl-*sn*-glycero-3-phosphocholine (DPPC), the tails of which contain 14 and 16 carbons, respectively. These lipids were chosen due to ease of vesicle formation under the conditions employed in this study[23] and the tendency of phosphatidylcholine lipid bilayers to be tolerant of added components with respect to maintenance of their microheterogeneous structures.[24] Lipid bilayers composed of DMPC have thicknesses on the order of ∼31−34 Å, while DPPC lipid bilayers are slightly thicker (∼34−37 Å).[25] The thickness of DMPC and DPPC bilayer membranes is close to the molecular lengths of **DSBN+** and **DSSN+** (∼35−40 Å).

(18) (a) Johnsen, M.; Paterson, M. J.; Arnbjerg, J.; Christiansen, O.; Nielsen, C. B.; Jørgensen, M.; Ogilby, P. R. *Phys. Chem. Chem. Phys.* **2008**, *10*, 1177–1191. (b) Meier, H. *Angew. Chem., Int. Ed.* **2005**, *44*, 2482–2506. (c) Narwark, O.; Gerhard, A.; Meskers, S. C. J.; Brocke, S.; Thorn-Csányi, E.; Bässler, H. *Chem. Phys.* **2003**, *294*, 17–30. (d) Seixas de Melo, J.; Burrows, H. D.; Svensson, M.; Andersson, M. R.; Monkman, A. P. *J. Chem. Phys.* **2003**, *118*, 1550–1556.

(19) (a) Pond, S. J. K.; Rumi, M.; Levin, M. D.; Parker, T. C.; Beljonne, D.; Day, M. W.; Brédas, J.-L.; Marder, S. R.; Perry, J. W. *J. Phys. Chem. A* **2002**, *106*, 11470–11480. (b) Renak, M. L.; Bartholomew, G. P.; Wang, S. J.; Ricatto, P. J.; Lachicotte, R. J.; Bazan, G. C. *J. Am. Chem. Soc.* **1999**, *121*, 7787–7799. (c) Rumi, M.; Ehrlich, J. E.; Heikal, A. A.; Perry, J. W.; Barlow, S.; Hu, Z.; McCord-Maughon, D.; Parker, T. C.; Rockel, H.; Thayumanavan, S.; Marder, S. R.; Beljonne, D.; Brédas, J.-L. *J. Am. Chem. Soc.* **2000**, *122*, 9500–9510. (d) Wang, S. J.; Oldham, W. J.; Hudack, R. A.; Bazan, G. C. *J. Am. Chem. Soc.* **2000**, *122*, 5695–5709.

(20) Gaylord, B. S.; Wang, S.; Heeger, A. J.; Bazan, G. C. *J. Am. Chem. Soc.* **2001**, *123*, 6417–6418.

(21) (a) Hsu, J.-H.; Fann, W.; Chuang, K.-R.; Chen, S.-A. *Proc. SPIE* **1997**, *3145*, 436–443. (b) Je, J.; Kim, O.-K. *Macromol. Symp.* **2007**, *249−250*, 44–49.

(22) (a) Marques, E. F. *Langmuir* **2000**, *16*, 4798–4807. (b) Robinson, J. N.; Cole-Hamilton, D. J. *Chem. Soc. Rev.* **1991**, *20*, 49–94.

(23) (a) Ref 22. (b) Knoll, W.; Ibel, K.; Sackmann, E. *Biochemistry* **1981**, *20*, 6379–6383. (c) Morigaki, K.; Walde, P. *Curr. Opin. Colloid Interface Sci.* **2007**, *12*, 75–80. (d) Šegota, S.; Težak, Đ. *Adv. Colloid Interface Sci.* **2006**, *121*, 51–75. (e) Singer, M. A.; Finegold, L.; Rochon, P.; Racey, T. J. *Chem. Phys. Lipids* **1990**, *54*, 131–146. (f) Woodle, M. C.; Papahadjopoulos, D. *Methods Enzymol.* **1989**, *171*, 193–217.

(24) Steinberg-Yfrach, G.; Rigaud, J.-L.; Durantini, E. N.; Moore, A. L.; Gust, D.; Moore, T. A. *Nature* **1998**, *392*, 479–482.

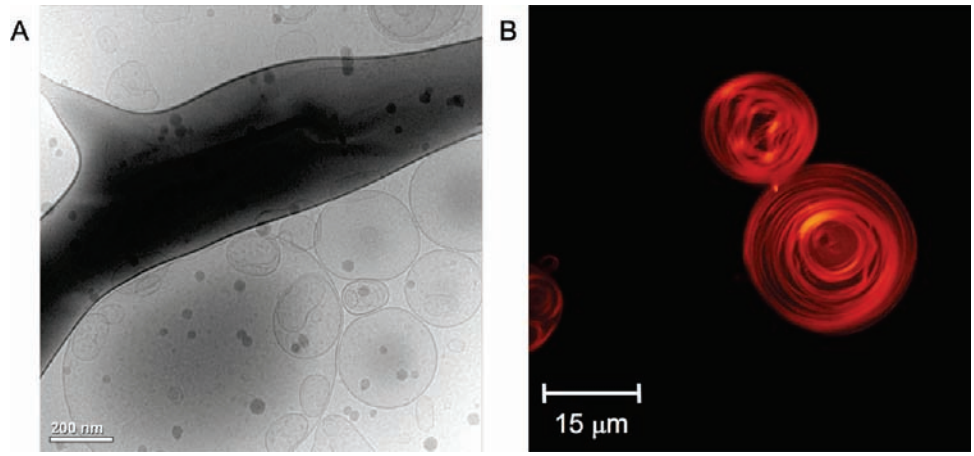

Figure 3. (A) Cryo-TEM image of unilamellar DMPC vesicles modified with 5 mol % of **DSBN**+ relative to lipid (16 mg/mL). (B) Confocal microscopy image of 5 mol % of **DSBN**+/DMPC multilamellar vesicles (2 mg/mL) obtained following 488 nm excitation. Each image demonstrates successful vesicle formation as well as a maintained liposomal microstructure upon addition of **DSBN**+. The confocal microscopy image is generated by the fluorescence response of **DSBN**+ and demonstrates oligoelectrolyte association with lipid bilayers.

Such similarities were anticipated to favor the type of membrane intercalation shown in Figure 1.

Efforts to modify the vesicle membranes with **DSBN**+ and **DSSN**+ followed modified literature procedures.[26] First, a lipid stock solution containing the desired fraction of either **DSSN**+ or **DSBN**+, typically 1−5 mol % relative to lipid, was prepared in methanol. This lipid/COE stock solution was then heated and held above the transition temperature of the lipid (23 and 41 °C for DMPC and DPPC, respectively) as the solvent was removed via Argon flushing, followed by vacuum drying to a constant weight. The resulting lipid/COE solid was then suspended in pH = 7.3 HEPES buffer to the desired concentration (1−10 mg/mL). Multilamellar vesicles were then formed by self-assembly upon sonication of the resulting solution. Unilamellar vesicles were prepared by filtration (using 0.45 or 0.2 μm pore size syringe filters) or by extrusion.[27]

Confirmation of vesicle formation and that the microheterogeneous liposomal structure is maintained upon modification with **DSBN**+ or **DSSN**+ was provided by cryogenic transmission electron microscopy (cryo-TEM) and confocal microscopy. The cryo-TEM image of unilamellar DMPC vesicles containing membrane embedded **DSBN**+ shown in Figure 3A demonstrates successful vesicle formation, as well as unperturbed liposomal microstructure. Figure 3B is a confocal microscopy image of multilamellar DMPC vesicles prepared in the presence of **DSBN**+. The image was generated by **DSBN**+ fluorescence emission following excitation at 488 nm. The layers that compose the vesicles can be seen, demonstrating that these oligoelectrolytes readily associate with the membranes. Subsequent characterization described in more detail below will demonstrate that, indeed, the chromophores span the width of the membranes.

Optical Characterization of PV Oligoelectrolytes within Lipid Bilayers. Several indicative changes in UV−vis and PL properties of **DSSN**+ and **DSBN**+ are observed upon association with phospholipid bilayer membranes. A comparison of the UV−vis and PL spectra of **DSSN**+ and **DSBN**+ in water and lipid bilayers is shown in Figure 4; the corresponding summary of the data is provided in Table 2. Compared to the spectroscopic features of the chromophores in water, one observes a bathochromic shift in λ_{abs} (21 and 16 nm for **DSSN**+ and **DSBN**+, respectively) and a large hypsochromic shift in λ_{em} (62 and 92 nm for **DSSN**+ and **DSBN**+, respectively) when associated with the lipid bilayers. Each shift is accompanied by the appearance of vibronic structure. When compared to the

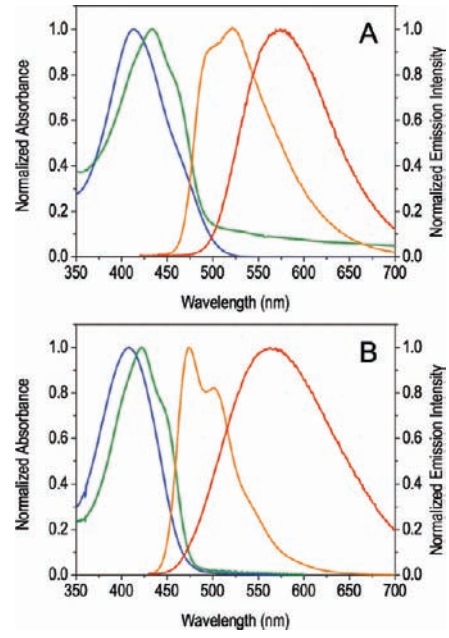

Figure 4. Normalized UV−vis absorbance and PL spectra of (A) **DSSN**+ and (B) **DSBN**+ in pH 7.3 HEPES buffer (absorbance = blue, emission = red) and while embedded within DMPC vesicle membranes (absorbance = green, emission = orange). Both molecules exhibit an indicative red shift in λ_{abs} (21 and 16 nm for **DSSN**+ and **DSBN**+, respectively) and a blue shift in λ_{em} (62 and 92 nm for **DSSN**+ and **DSBN**+, respectively) due to the difference in environmental polarity between an aqueous solvent and the inner region of a lipid bilayer.

(25) (a) Kučerka, N.; Uhríková, D.; Teixeira, J.; Balgavý, P. *Phys. B: Condens. Matter* **2004**, *350*, e639−e642. (b) Lewis, B. A.; Engelman, D. M. *J. Mol. Biol.* **1983**, *166*, 211–217.
(26) Lin, A. J.; Slack, N. L.; Ahmad, A.; George, C. X.; Samuel, C. E.; Safinya, C. R. *Biophys. J.* **2003**, *84*, 3307–3316.
(27) (a) Olson, F.; Hunt, C. A.; Szoka, F. C.; Vail, W. J.; Papahadjopoulos, D. *Biochim. Biophys. Acta* **1979**, *557*, 9–23. (b) Socaciu, C.; Bojarski, P.; Aberle, L.; Diehl, H. A. *Biophys. Chem.* **2002**, *99*, 1–15. (c) Szoka, F.; Olson, F.; Heath, T.; Vail, W.; Mayhew, E.; Papahadjopoulos, D. *Biochim. Biophys. Acta* **1980**, *601*, 559–571.

Table 2. Comparison of UV−vis Absorbance and PL Spectroscopy of **DSSN**+ and **DSBN**+ in Water and Lipid Bilayers

	water		lipid bilayer	
	$\lambda_{abs}(\varepsilon_{max})^a$	$\lambda_{em}(\eta)^b$	$\lambda_{abs}(\varepsilon_{max})$	$\lambda_{em}(\eta)$
DSSN+	412 (6.6)	594 (0.06)	433 (8.4)	532 (0.85)
DSBN+	406 (6.0)	566 (0.33)	422 (4.8)	474 (0.59)

[a] ε_{max} values are reported in units of L mol^{-1}cm^{-1} × 10^{-4}. [b] η values were obtained relative to a fluorescein standard at pH 12.

emission features of each chromophore in toluene (Figure 2), it can be seen that the emission of **DSSN**+ and **DSBN**+ within lipid bilayer membranes is consistent with a nonpolar environment. The ε_{max} and η values of **DSSN**+ and **DSBN**+ embedded in lipid bilayers (8.4 and 4.8 L mol^{-1}cm^{-1} × 10^{-4} for ε_{max}, and 0.85 and 0.59 for η of **DSSN**+ and **DSBN**+, respectively) are greater than those of these chromophores in water (6.6 and 6.0 L mol^{-1}cm^{-1} × 10^{-4} for ε_{max}, and 0.06 and 0.33 for η of **DSSN**+ and **DSBN**+, respectively), with the exception of the ε_{max} of **DSBN**+. These values are also approaching the characteristic values in toluene (10.7 and 8.4 L mol^{-1}cm^{-1} × 10^{-4} for ε_{max}, and 0.95 and 0.98 for η of **DSSN** and **DSBN**, respectively). The observed UV−vis and PL features of **DSSN**+ and **DSBN**+ indicate that these chromophores are embedded within the lipid bilayers and experience the more hydrophobic interior environment of the membrane.[28]

Figure 5 displays four confocal microscopy images of modified multilamellar vesicles, each corresponding to one of the four lipid/oligoelectrolyte combinations (DMPC/**DSBN**+, DPPC/**DSBN**+, DMPC/**DSSN**+, and DPPC/**DSSN**+; each 5 mol % of COE). These images, obtained following excitation of the chromophores, illustrate preferential accumulation inside the vesicle membranes. These images also suggest excellent structural diversity; i.e., the short/long COEs can both be incorporated into bilayers composed of lipids of varying tail lengths.

Oligoelectrolyte Molecular Orientation within Lipid Bilayers. Molecular orientations of **DSBN**+ and **DSSN**+ were probed via confocal microscopy by examination of the emission intensity profile of the COEs within stationary vesicles following excitation using a polarized source. Oligo(phenylenevinylenes) possess a primary transition dipole (μ) that is oriented along the long molecular axis.[29] The probability of generating an emissive excited state using a polarized excitation source depends on the orientation of μ with respect to the plane of polarization of the excitation light.[30] An immobilized membrane with **DSBN**+ or **DSSN**+ in the expected molecular orientation should exhibit regions with greater and less emission upon excitation with a polarized excitation source. This concept has been previously employed to investigate local order in smectic liquid crystals.[31]

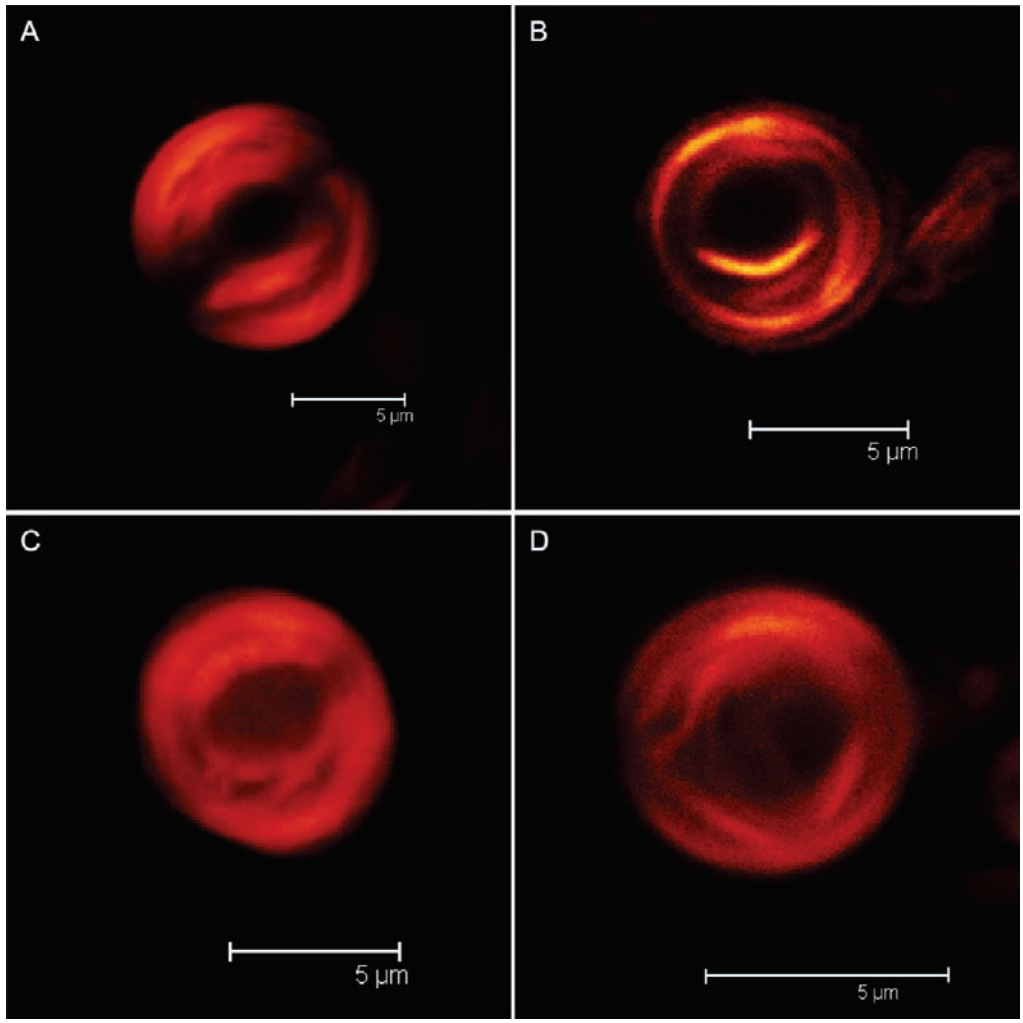

Figure 5. Confocal microscopy fluorescence images of multilamellar vesicles containing 5 mol % of oligoelectrolyte (10 mg/mL). (A) DMPC/**DSBN**+. (B) DPPC/**DSBN**+. (C) DMPC/**DSSN**+. (D) DPPC/**DSSN**+. Images were collected by excitation at 488 nm.

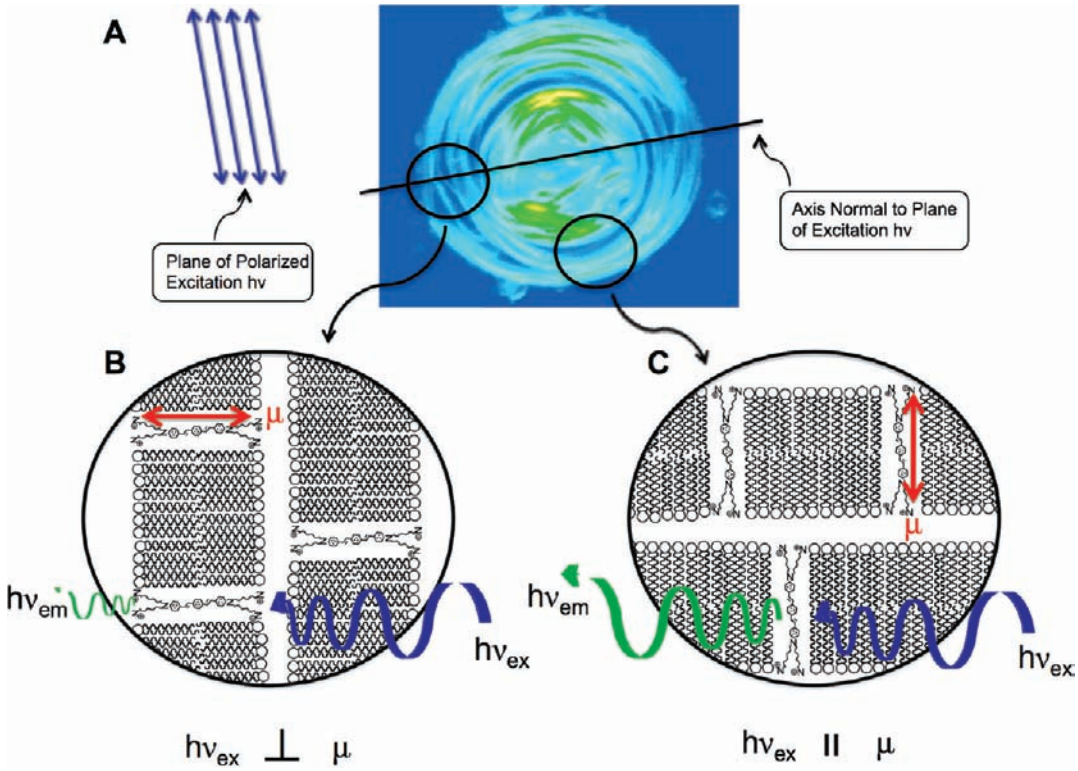

Figure 6. (A) Image of a stationary multilamellar DMPC vesicle (diameter = ~15 μm) containing 3 mol % of **DSBN**+ that exhibits an equatorial extinction line (black line) perpendicular to the plane of the 488 nm Ar laser excitation light. (B) A closer view within the extinction line region in which **DSBN**+ molecules are oriented with their transition dipoles (denoted by red arrows) perpendicular to the plane of the excitation light (blue arrow) resulting in attenuated emission (small green arrow). (C) A closer view within the regions above and below the extinction line in which **DSBN**+ transition dipoles are oriented parallel to the plane polarized excitation light (blue arrow) resulting in a greater number of excited states and stronger emission (larger green arrow).

Figure 6A provides the confocal fluorescence image of a stationary vesicle obtained upon excitation of membrane-embedded **DSBN**+ with a polarized excitation source. The vesicle image contains an equatorial region (highlighted by a black line) with attenuated intensity perpendicular to the plane of the polarized light. These intensity distributions can be used to determine the preferred orientations of μ. Specifically, less intense emission is anticipated in regions where μ is perpendicular to the plane of polarized excitation light, as illustrated in Figure 6B. Conversely, as shown in Figure 6C, the alignment of chromophores such that μ is parallel to the plane of incident polarized light favors excitation, leading to greater emission intensity. In Figures 6B and 6C, the emission output is schematically represented by the size of the green arrows. The results indicate that **DSBN**+ and **DSSN**+ exist within lipid bilayers in an ordered orientation with the long axis perpendicular to the plane of the membrane. This molecular orientation is fully consistent with the integration of π-segments and polar groups as shown in Figure 1.

Transmembrane Electron Transport. OPVs within a saturated alkane thiol monolayer can facilitate charge tunneling from a metallic electrode to a tethered redox species.[9] We have chosen a variation of this approach in which supported bilayer membranes (sBLM) containing **DSSN**+, **DSBN**+, and other control molecules were prepared on the surface of a glassy carbon electrode surface. The sBLM-modified electrodes were then employed in a series of "blocking" experiments in which cyclic voltammetry was used to monitor the reversible oxidation of aqueous ferricyanide. The unmodified sBLM acts as an insulating layer between the working electrode and the solution containing ferricyanide thereby greatly suppressing the redox current.[32] **DSBN**+ and **DSSN**+ within an sBLM are oriented with their long axes perpendicular to the surface of the electrode, thus potentially forming a transmembrane molecular wire through which electrons tunnel to and from redox species at the water−membrane interface.

In our experiments, a bare glassy carbon electrode and glassy carbon electrodes supporting DMPC and DPPC BLMs containing no additional components, 2 mol % of tridodecylamine (TDA), 2 mol % of **DSSN**+, and 2 mol % of **DSBN**+ (relative to lipid) were used to collect voltammograms in the presence of an aqueous 0.5 M KCl solution containing 2 mM ferricyanide. The surface of the electrode was pretreated, according to literature protocols, to promote bilayer formation.[33] Specifically,

(28) Bose, D.; Ghosh, D.; Das, P.; Girigoswami, A.; Sarkar, D.; Chattopadhyay, N. *Chem. Phys. Lipids* **2010**, *163*, 94–101.
(29) (a) Gierschner, J.; Ehni, M.; Egalhaaf, H.-J.; Medina, B. M.; Beljonne, D.; Benmansour, H.; Bazan, G. C. *J. Chem. Phys.* **2005**, *123*, 144914. (b) Spano, F. C. *Chem. Phys. Lett.* **2000**, *331*, 7–13.
(30) (a) Bur, A. J.; Roth, S. C.; Thomas, C. L. *Rev. Sci. Instrum.* **2000**, *71*, 1516–1523. (b) Bur, A. J.; Lowry, R. E.; Roth, S. C.; Thomas, C. L.; Wang, F. W. *Macromolecules.* **1992**, *25*, 3503–3510.
(31) Smalyukh, I. I.; Shiyanovskii, S. V.; Lavrentovich, O. D. *Chem. Phys. Lett.* **2001**, *336*, 88–96.
(32) (a) Wiegand, G.; Arribas-Layton, N.; Hillebrandt, H.; Sackmann, E.; Wagner, P. *J. Phys. Chem. B.* **2002**, *106*, 4245–4254. (b) Żebrowska, A.; Krysiński, P.; Łotowski, Z. *Bioelectrochemistry* **2002**, *56*, 179–184.
(33) (a) Huang, W.; Zhang, Z.; Han, X.; Tang, J.; Wang, J.; Dong, S.; Wang, E. *Biophys. J.* **2002**, *83*, 3245–3255. (b) Wu, Z.; Tang, J.; Cheng, Z.; Yang, X.; Wang, E. *Anal. Chem.* **2000**, *72*, 6030–6033.

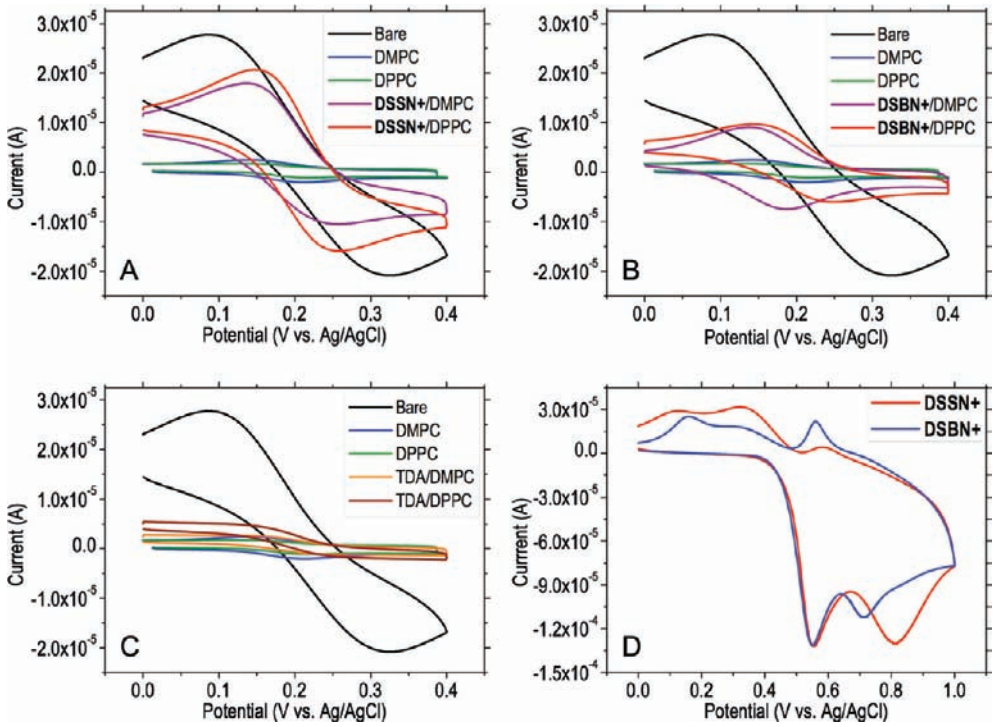

Figure 7. (A−C) Results of the cyclic voltammetry blocking experiment that indicate that **DSSN**+ (A) and **DSBN**+ (B) facilitate transmembrane electron transport across insulating sBLMs from the glassy carbon electrode surface to aq ferricyanide. The insulating effect can be seen by comparison of the prevalent reversible redox couple observed when a bare electrode is employed (A−C, black curves) that is absent in the traces obtained using electrodes supporting unmodified BLMs (A−C, blue and green curves for DMPC and DPPC sBLMs, respectively). The facilitation of electron transport by **DSSN**+ and **DSBN**+ can be seen by the greater current observed when an electrode bearing an sBLM containing 2 mol % of **DSSN**+ or **DSBN**+ is employed (red and purple curves for DMPC and DPPC modified sBLMs, respectively). Little to no transmembrane electron transfer occurs across an sBLM containing 2 mol % of TDA (C, orange and dark red traces for modified DMPC and DPPC sBLMs). (D) Current/potential curves corresponding to **DSSN**+ and **DSBN**+ show an oxidation (∼0.55 V vs Ag/AgCl) above that of ferricyanide (∼0.3 V vs Ag/AgCl). These data suggest a charge tunneling process. All traces shown were obtained using a 200 mV/s scan rate.

membranes were prepared by depositing 3 μL of a 2 mg/mL lipid stock solution containing either 0 or 2 mol % of **DSSN**+, **DSBN**+, or TDA onto a surface modified electrode, followed by submerging into pH 7.4 phosphate buffer to allow sBLM formation. The sBLM containing TDA provides a control sample to examine whether additional membrane components and possible structural modifications increase electron transfer to redox species in solution.

Figure 7 shows the results of the sBLM blocking experiments. The reversible ferricyanide oxidation ($E_{p(ox)} = 0.252$ V vs SCE) is observed in the voltammogram obtained by using a bare glassy carbon electrode (A−C, black curves). The insulating property of an unmodified sBLM is confirmed by nearly featureless CV traces (Figure 7A−C, blue and green curves). Similarly, the CV traces obtained employing an electrode supporting a BLM containing 2 mol % of TDA is also featureless (Figure 7C), evidence that the presence of this component does not perturb the bilayer structure.

CV traces corresponding to sBLMs modified with **DSSN**+ and **DSBN**+ (Figure 7A and 7B, purple and red for modified DMPC and DPPC sBLMs, respectively) display higher currents with respect to the control experiments, indicating that transmembrane electron transfer is facilitated. That observed oxidation occurs at $E_{p(ox)} = \sim 0.3$ V vs Ag/AgCl and $E_{p(red)} = \sim 0.1$ V vs Ag/AgCl (Figure 7A−C), below the oxidation potential of **DSSN**+ and **DSBN**+ (Figure 7D, $E_{ox} = \sim 0.55$ V), suggests a transmembrane tunneling process. The ability of **DSSN**+ to better facilitate transmembrane electron transport can be seen by the greater current response corresponding to runs employing sBLMs containing **DSSN**+ (Figure 7A) instead of **DSBN**+ (Figure 7B). This higher current may be attributed to the ability of **DSSN**+ to more completely span the membrane structure due to its more extended conjugation length.

The results obtained from the CV blocking experiments indicate that transmembrane charge transfer through insulating sBLMs is facilitated upon incorporation of **DSSN**+ and **DSBN**+. Furthermore, these COEs may act as "molecular wire" tunneling pathways.

Interaction with Living Systems. Up to this point, only the interaction of these COEs with artificial membranes has been discussed. We now examine interactions with living microorganisms. Our studies focused on yeast due to its application as an exoelectrogen in microbial fuel cells (see next section). Figure 8 consists of two sets of confocal microscopy fluorescence images of Baker's yeast, each stained and imaged in a 100 μM solution of **DSSN**+ (Figure 8A) or **DSBN**+ (Figure 8B) after 1 h of shaking *without* exchanging the staining media. These images illustrate the apparent preferential accumulation of the COEs within cell membranes, in agreement with other reports in which amphiphilic compounds are introduced to living systems.[34] The lack of background fluorescence is attributed to the low η of these chromophores when in contact with water.

COE Electron Transport Mediators in Yeast Microbial Fuel Cells. Microbial fuel cells (MFCs) function on the principle that electrons from the metabolic cycle of many anaerobic and facultative organisms known as exoelectrogens can be used to

(34) Reeve, J. E.; Collins, H. A.; Mey, K. D.; Kohl, M. M.; Thorley, K. J.; Paulsen, O.; Clays, K.; Anderson, H. L. *J. Am. Chem. Soc.* **2009**, *131*, 2758–2759.

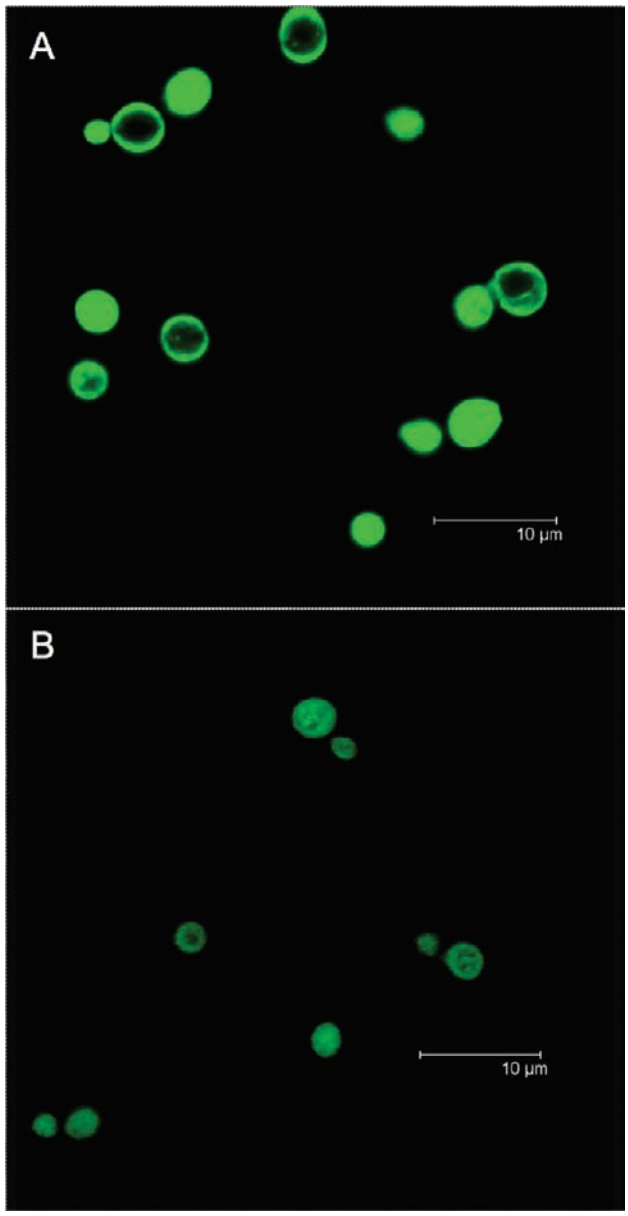

Figure 8. Confocal microscopy fluorescence images of Baker's yeast stained with 100 μM **DSSN**+ (A) and **DSBN**+ (B) upon excitation at 488 nm. It can be seen that these dyes readily interact with the membranes of living cells. Note that some cells (that are imaged in the focal plane) possess the equatorial extinction line that indicates an ordered molecular orientation within cell membranes.

generate a useful electrical current.[35] Recent work has shown that a surprisingly large number of organisms exhibit exoelectrogenic character.[36] Extracting energy from these organisms is typically achieved by using a strategy similar to that employed in a chemical fuel cell. Typically, a community of microorganisms populating a high surface area electrode in an anaerobic environment oxidize biological fuels such as sugars in an anode compartment. This anode compartment is commonly separated from a cathode compartment by a proton exchange membrane

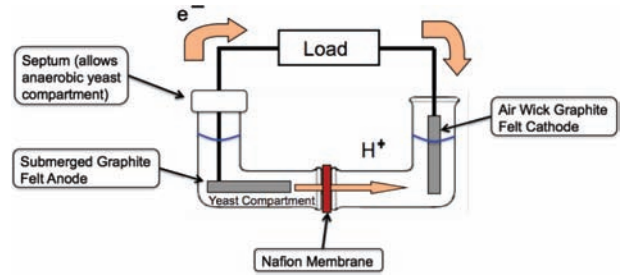

Figure 9. Schematic of the U-tube MFC design[40] employed in this study. The MFC is composed of an anaerobic anode/yeast compartment that is separated by a proton permeable Nafion membrane from an aerobic cathode compartment.

that maintains charge balance, much like a salt bridge in a galvanic cell. The cathode compartment is typically aerobic and is the site of oxygen reduction, which completes the oxidation−reduction reaction of the whole cell. Electrons gained from biofuel oxidation at the anode must flow through a desired pathway (the lead between the electrodes) to participate in oxygen reduction at the cathode, thus generating a usable current.[37] In summary, biological fuel is oxidized by the microorganisms, releasing electrons to the anode and protons to the solution. Protons diffuse into the cathode compartment, where they participate in oxygen reduction at the cathode to form water.[38] A schematic of a U-tube type MFC that outlines the key compartments and components is shown in Figure 9. Although the MFC concept is relatively simple, much remains poorly understood about the factors that influence their performance at the molecular, cellular, and device level.[39]

Some exoelectrogens are capable of direct electron transfer to an electrode, while others require an electron transport mediator.[41] Common mediators employed in bacterial and yeast fuel cells are diffusion-based redox carriers that are membrane permeable, such as methylene blue and neutral red.[42] These types of mediators may have undesirable features, such as cellular uptake that does not favor electron transfer, redox properties that are not compatible with target species and substrates,[43] and possible diffusion limited kinetics.[44] It would thus be beneficial to modify microorganisms with structural features that enable transmembrane electron transport and that do not impede their metabolic function. The accumulated information on **DSSN**+ and **DSBN**+ argues that these molec-

(35) (a) Logan, B. E. *Nat. Rev. Microbiol.* **2009**, *7*, 375–381. (b) Schaetzle, O.; Barriere, F.; Baronian, K. *Energy Environ. Sci.* **2008**, *1*, 607–620.

(36) (a) Ref 35. (b) Logan, B. E.; Regan, J. M. *Trends Microbiol.* **2006**, *14*, 512–518. (c) Lovley, D. R. *Nat. Rev. Microbiol.* **2006**, *4*, 497–508.

(37) (a) Ref 35. (b) Walker, A. L.; Walker, C. W., Jr. *J. Power Sources* **2006**, *160*, 123–129.

(38) Logan, B. E.; Hamelers, B.; Rozendal, R.; Schröder, U.; Keller, J.; Freguia, S.; Aelterman, P.; Verstraete, W.; Rabaey, K. *Environ. Sci. Technol.* **2006**, *40*, 5181–5192.

(39) (a) Logan, B. E.; Regan, J. M. *Environ. Sci. Technol.* **2006**, *40*, 5172–5180. (b) Yazdi-Rismani, H.; Carver, S. M.; Christy, A. D.; Tuovinen, O. H. *J. Power Sources* **2008**, *180*, 683–694. (c) Zhao, F.; Slade, R. C. T.; Varcoe, J. L. *Chem. Soc. Rev.* **2009**, *38*, 1926–1939.

(40) (a) Milliken, C. E.; May, H. D. *Appl. Microbiol. Biotechnol.* **2007**, *73*, 1180–1189. (b) Sund, C. J.; Wong, M. S.; Sumner, J. J. *Biosens. Bioelectron.* **2009**, *24*, 3144–3147. (c) Sund, C. J.; McMasters, S.; Crittenden, S. R.; Harrell, L. E.; Sumner, J. J. *Appl. Microbiol. Biotechnol.* **2007**, *76*, 561–568.

(41) Watanabe, K.; Manefield, M.; Lee, M.; Kouzuma, A. *Curr. Opin. Biotechnol.* **2009**, *20*, 633–641.

(42) Gunawarddena, A.; Fernando, S.; To, F. *Int. J. Mol. Sci.* **2008**, *9*, 1893–1907.

(43) Wilkinson, S.; Klar, J.; Applegarth, S. *Electroanalysis* **2006**, *18*, 2001–2007.

(44) (a) Bullen, R. A.; Arnot, T. C.; Lakeman, J. B.; Walsh, F. C. *Biosens. Bioelectron.* **2006**, *21*, 2015–2045. (b) Torres, C. I.; Marcus, A. K.; Lee, H.-S.; Parameswaran, P.; Krajmalnik-Brown, R.; Rittmann, B. E. *FEMS Microbiol. Rev.* **2010**, *34*, 3–17.

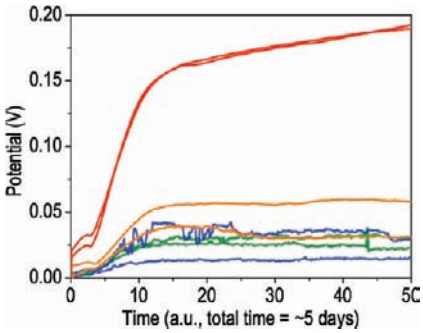

Figure 10. Plots of yeast MFC voltage production as a function of time for MFCs containing no mediator (green), 13 μM methylene blue (blue), 190 nM **DSBN**+ (orange), and 190 nM **DSSN**+ (red). Voltage values are obtained by measuring the potential across a 10 kΩ resistor. Note the large increase in performance afforded by **DSSN**+ despite a concentration 2 orders of magnitude lower than that of the common diffusion-based electron transport mediator methylene blue.

ular species display all the desirable features to accomplish this modification.

A U-tube type MFC[40] (Figure 9) was employed to test and compare the performance of a series of yeast MFCs employing nanomolar concentrations of **DSSN**+ and **DSBN**+ to the performance of a series of negative controls with no external mediator and a series of positive controls employing the common electron transport mediator methylene blue in micromolar concentrations. The details of MFC construction, preparation, and evaluation are discussed in detail in the Experimental Section (Supporting Information), but it is important to note here that MFC performance is evaluated in terms of voltage instead of current. Voltage readings were obtained by measuring the potential across a 10 kΩ resistor.[38,40b]

Figure 10 shows the relative performance of the tested MFCs. Maximum voltages (V_{max}) obtained for the mediator-less MFCs and those employing 13 μM methylene blue are ~25 mV (green) and ~40 mV (blue), respectively. MFCs employing the shorter oligoelectrolyte **DSBN**+ (190 nM) produce slightly greater voltages (V_{max} = ~55 mV, orange plots). A notable increase in performance is afforded by the longer **DSSN**+ (190 nM), which resulted in a ~5-fold increase in voltage production (V_{max} = ~200 mV) compared to methylene blue, despite being 2 orders of magnitude lower in concentration. Furthermore, the difference in performance between MFCs employing **DSSN**+ and **DSBN**+ is consistent with the difference in transmembrane electron transport properties observed in the cyclic voltammetry experiments.

The ability of **DSBN**+ and **DSSN**+ to be passed on to or exist within cell membranes of subsequent yeast generations born over the course of MFC operation was also investigated. Aliquots of an MFC using the mediator **DSSN**+ were taken before MFC inoculation and after 4 days of MFC operation. Cells from each of these aliquots were imaged using a confocal microscope in epi-fluorescence mode and brightfield mode. Figure 11A corresponds to the yeast sample containing 25 μM **DSSN**+ that was used to inoculate the MFC series corresponding to this mediator. This particular staining/cell membrane modification procedure consisted of light shaking for 3 h in the presence of micromolar oligomer concentrations. The external cell membranes are observable due to emission of **DSSN**+. Figure 11B is an epi-fluorescence and brightfield image (inset, lower left) of a small group of yeast cells removed from the same MFC on the fourth day of operation. These images were collected using the same setup as the images in Figure 11A

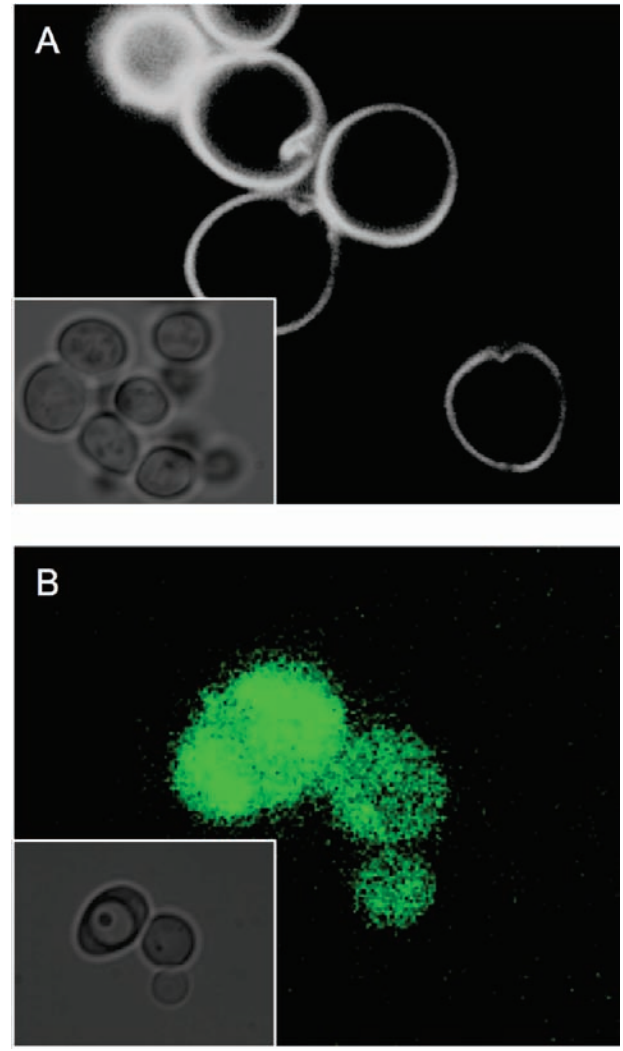

Figure 11. (A) Epi-fluorescence image of yeast in growth media containing 25 μM **DSSN**+ prior to fuel cell inoculation. The yeast is stained such that the primarily cell membranes can be seen. Inset: example brightfield image of the sample prior to inoculation. (B) Epi-fluorescence image of yeast removed from the MFC on day 4 of operation. Although emission is not very intense, these cells contain **DSSN**+ despite the large dilution upon inoculation (to a nanomolar regime) and exponential increase in the number of total cells over the course of 4 days. Inset: Brightfield image that matches the day 4 epi-fluorescence image. Note: λ_{ex} = ~480 nm provided by a Hg lamp and the proper filter. This excitation range is out of the range of absorbance of the fluorescent amino acids tryptophan, tyrosine, and phenylalanine (λ_{abs}(Trp, Tyr, Phe) = ~220−320 nm), thus any observed emission is attributed to **DSSN**+.

and demonstrate the presence of this mediator in later cell generations. The emission is much less intense, an effect that is not surprising considering the exponentially greater number of cells present after 4 days of cell reproduction. This result indicates that **DSSN**+ can be passed on to daughter cells either during budding reproduction (implying that some cellular uptake, into cytoplasm, occurs) and/or by an equilibrium between membrane embedded and aqueous **DSSN**+.

Conclusion

To summarize, we have demonstrated the incorporation of **DSBN**+ and **DSSN**+ within membranes. Insertion of the two oligoelectrolytes changes the optical and electronic properties of the resulting modified membranes. Additionally, the solvatochromic features of these chromophores can be used to probe

their location and the polarity of the medium. The size and relative positions of the charges and hydrophobic regions of **DSBN**+ and **DSSN**+ led us to propose the intuitive, ordered molecular organization shown in Figure 1. This supramolecular arrangement, in which the rigid π-conjugated region lies within the inner membrane oriented such that the long molecular axis is normal to the bilayer plane, was confirmed by confocal microscopy using a polarized excitation source. We find two important consequences of integrating molecules such as **DSBN**+ and **DSSN**+. First, the optical properties and affinity of these chromophores for both synthetic and biological membranes allow for effective fluorescence imaging of living organisms. It is also worth noting that large two-photon cross sections imply that these compounds can be applied to three-dimensional imaging of biological samples. Second, all the evidence accumulated thus far is consistent with facilitation of cross-membrane charge transport by these conjugated oligo-electrolytes. It is tempting to hypothesize here that the mechanism is charge tunneling by virtue of the rigid π-structure. In other words, **DSBN**+ and **DSSN**+ do not serve as simple shuttles. Observations that (a) there is affinity for the membranes of living organisms and (b) that transmembrane electron transfer is facilitated led us to consider that the current generation in microbial fuel cells could be improved by the addition of **DSBN**+ and **DSSN**+. We envisioned their function as mediators that transfer electrons from within the organism to the electrode. This idea was confirmed by the nearly 5-fold increase in performance of yeast microbial fuel cells afforded by using **DSSN**+ compared to that of the common diffusion-based electron transport mediator methylene blue, despite 2 orders of magnitude difference in concentration. These findings not only are of potential impact within the scope of contacting microorganisms with electrode surfaces but also open the possibilities of intercellular electronic communication.

Acknowledgment. The authors thank the Institute for Collaborative Biotechnologies (W911F-09-D-0001), Air Force Office of Scientific Research (FA9550-08-1-0248), and the National Science Foundation (DMR0606414, and subcontract from Caltech: CMMI-0730689) for financial support; Mr. Htet Khant for cryo-TEM imaging; Dr. Alexander Mikhailovsky for assistance with photophysical measurements; Dr. Joshua M. Kogot for cell cultures and helpful consultations; and Dr. Myung Chul (MC) Choi for stimulating discussions that contributed to this work.

Supporting Information Available: Experimental details for synthesis, vesicle and supported lipid bilayer preparation, cyclic voltammetry measurements, cell staining, confocal fluorescence and cryo-TEM imaging, microbial fuel cell preparation, instrumentation, and complete reference 14. This material is available free of charge via the Internet at http://pubs.acs.org.

JA1016156